

# Constrained Predictive Control of Helicopters

## Abstract

**Purpose** – The purpose of this paper is to show the feasibility of constrained model predictive control (MPC) for sophisticated helicopter models which are derived by physical considerations.

**Approach** – Physics based modeling is used to create control oriented helicopter models. Advanced constrained controllers are designed and tested for these sophisticated models.

**Findings** – The helicopter models are valid and constrained MPC shows considerable promise for robust tracking.

**Practical implications** – MPCs can be implemented for highly constrained helicopter flights.

**Originality/value** – A complete process of control oriented, physics based model development for helicopters followed by MPC design is developed. It is also proved that constrained MPC can be used and implemented online to robustly track discontinuous helicopter trajectories with heterogeneous constraints, even when the models are sophisticated and physics based.

**Keywords** Constrained Control, Model Predictive Control, Physics Based Helicopter Modeling, Discontinuous Trajectories.

**Paper type** Research paper

## Introduction

Historically, aerospace vehicles control was approached using a decoupling principle: a single rigid body model was considered sufficient and the equations of motion were assumed to decouple. This led to tremendous simplification, resulting in low order controllers. However, the decoupling approximation was soon found inadequate even for fixed wing aircraft, when inertial roll coupling was first analyzed in Phillips, 1948. Nevertheless, decoupling continued to be used because technological limitations placed severe restrictions on the dimension of controllers that could be implemented. For rotorcraft, the single rigid body and decoupling assumptions are crude approximations. Their relative success in helicopter control was due to very conservative designs, which are not suitable for multi-objective missions with conflicting requirements. Several publications actually advocate for the use of coupled, multibody models for rotorcraft control design (Sahasrabudhe et al., 1997a; Sahasrabudhe and Celi, 1997b).

The ideal situation is when the model used for control is physics-based and it captures the essential dynamics of interest through a process called “control oriented modeling”. In the first part of this paper we present the development of

such models for helicopters. Our models include a fully articulated main rotor, main rotor downwash, blade flexibility, fuselage and tail rotor aerodynamics. For control oriented modeling we use lumped system modeling for blade flexibility instead of solving nonlinear partial differential equations (PDEs) (Hodges and Dowell, 1974) or using finite element methods (Traugott et al., 2006). Our modeling approach, which involves application of the physics principles, *directly* leads to *finite* sets of ordinary differential equations (ODEs). This is a tremendous advantage because it facilitates direct use of modern, multivariable control theory. On the other hand if physics principles lead to PDEs models, only several ODEs are generated and retained to capture the dynamics of interest, amounting to qualitative *and* quantitative alteration of the original PDEs model. The models obtained using our approach consist indeed of nonlinear ODEs. The resulting models are validated by comparing their features (trim values and eigenvalues of linearized models) with results in the literature.

Control design is critical for safe and performant helicopter operation. Since helicopter flight is highly constrained, any control design should account for constraints on outputs and inputs. It is known that model predictive control (MPC) can simultaneously handle numerous output and input constraints (Maciejowski, 2001; Camacho and Bordons, 1999; Mayne et al., 2000). Therefore we design such controllers for models linearized around several flight conditions. The ability of MPC to track discontinuous trajectories while obeying heterogeneous constraints is investigated. Tracking discontinuous trajectories for helicopters is important because switching between flight conditions frequently occurs. For example, in the presence of atmospheric disturbances it may be required to switch from one attitude to another in order to better mitigate the disturbance.

Past research in MPC for helicopters focused predominantly on simple (Dutka et al., 2003; Afonso et al., 2010) or identified models (Bogdanov et al., 2001; Bottasso and Riviello, 2005; Dalamagkidis et al. 2010). On the other hand, our models are physics based, control oriented, and sufficiently complex to account for important effects in helicopter dynamics. **The feasibility of controlling helicopters using MPC was also recently investigated in Joeliando et al., 2011, where the focus was on a small-scale helicopter. In our paper we evaluate MPC for large scale helicopters (i.e. Puma SA 330) and the focus is on discontinuous trajectories.** We therefore design MPC for our models evaluating: a) ability to track discontinuous trajectories, b) satisfaction of heterogeneous constraints, c) computation time, d) robustness to modeling uncertainties.

## **Helicopter Model**

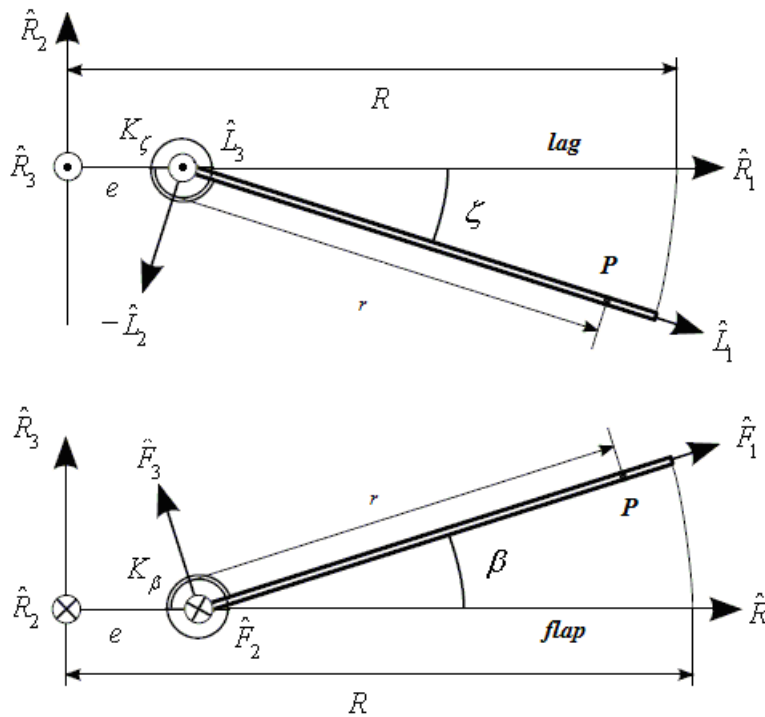
### **Modeling assumptions**

The Earth is inertially fixed and the atmosphere is stationary. The helicopter has a plane of symmetry, constant mass and constant inertia matrix. Linear incompressible aerodynamics is considered for each subsystem. Flapping, lead-lagging and flapwise bending angles are small.

### Newton-Euler equations, kinematic equations, and reference frames

The derivation of Newton-Euler and kinematic equations for the helicopter follows Padfield, 2007. The aircraft, hub, rotating, flapping, and lead-lagging reference frames and corresponding coordinate transformation matrices are described in Padfield, 2007; Done and Balmford, 2001 (see Figure 1 for flapping and lead-lagging).

**Figure 1** Flapping and Lead-Lagging



In Figure 1 blade flapping and lead-lagging motions are illustrated. In this Figure  $\beta$  and  $\zeta$  are flapping and lead-lagging angles,  $K_\beta$  and  $K_\zeta$  are stiffness coefficients of flapping and lead-lagging springs,  $e$  is hinge offset,  $r$  is blade strip distance from the flapping and lead-lagging hinge,  $R$  is blade radius, and  $\hat{F}_i, \hat{L}_i, \hat{R}_i$  are  $i$ -th unit vectors of flapping, lead-lagging and rotating frames, respectively.

### Single blade equations

Single blade equations are obtained by integrating infinitesimal aerodynamic and inertial moments acting on the blade strips along the blade span with respect to (w.r.t.) blade hinge and including lead-lagging spring and damper moments as well as flapping spring moment.

The absolute acceleration of a generic point  $P$  at position  $\vec{r}^P$  from the helicopter's center of gravity (cg) is

$$\vec{a}^{I-P} = \frac{d^2 \vec{r}^P}{dt^2} + \frac{d}{dt} (\vec{\omega}^{I-R} \otimes \vec{r}^P) + \vec{\omega}^{I-R} \otimes \left[ \frac{d \vec{r}^P}{dt} + \vec{\omega}^{I-R} \otimes \vec{r}^P \right] + \vec{a}_A \quad (1)$$

where  $\vec{\omega}^{I-R}$  is the angular velocity vector of rotating frame w.r.t. inertial frame,  $\vec{a}_A$  is the absolute acceleration of helicopter,  $\otimes$  is the vector product symbol,  $t$  is time. The reference frames,  $R$  (rotating) and  $I$  (inertial), are written as left superscripts. The position of  $P$  on the blade w.r.t. the cg in rotating frame, including flapping and lead-lagging motion, is

$$\vec{r}^P = [e + r \cos \beta \cos \zeta, -r \sin \zeta, h + r \sin \beta \cos \zeta]^T \quad (2)$$

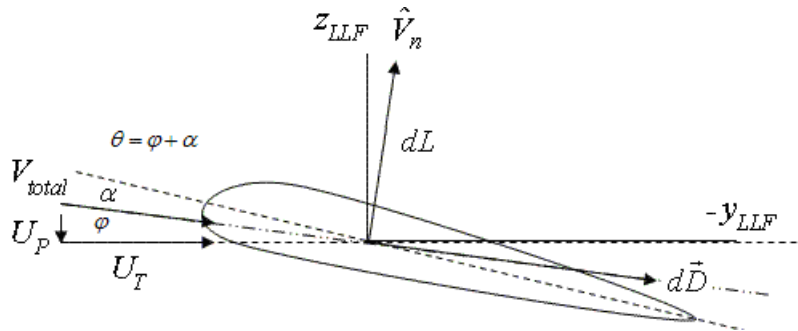
where  $h$  is the vertical distance from cg to main rotor hub and the left subscript represents the frame in which any quantity is written. Gravitational acceleration effect is ignored for blade equations, but included in the helicopter Newton-Euler equations. Using  $\vec{a}^{I-P}$  (Equation 1), the infinitesimal inertial force and moment are

$$d\vec{F}_I = -m \vec{a}^{I-P} dr, \quad d\vec{M}_I = \vec{r} \otimes d\vec{F}_I \quad (3)$$

where  $m$  is blade's linear mass density. The infinitesimal aerodynamic force and moment acting on a blade strip are determined using blade section angle of attack ( $\alpha$ ) and the oncoming air velocity of the blade strip ( $V_{air}$ ). The oncoming air velocity of the blade strip (Figure 2) in lead-lagging and flapping frame is

$$\vec{V}_{air}^{LLF} = [U_R, U_T, U_P]^T \quad (4)$$

**Figure 2** Blade Section-Infinitesimal Lift and Drag



Assuming: 1)  $U_T \gg U_P$  and  $U_R$  is ignorable, 2) drag coefficient is  $c_d = \delta_0 + \delta_2 \alpha^2$  (Dreier, 2007) where  $\delta_0$  and  $\delta_2$  are parasite and induced components, 3) lift coefficient is  $c_l = a_0 \alpha$  where  $a_0$  is the lift curve slope, the blade strip's infinitesimal lift and drag forces and  $\alpha$  are

$$dL = \frac{1}{2} \rho U_T^2 a_0 \alpha c dr, \quad dD = \frac{1}{2} \rho U_T^2 (\delta_0 + \delta_2 \alpha^2) c dr, \quad \alpha = \theta - \frac{U_P}{U_T} \quad (5)$$

where  $c$  is the blade chord length and the blade pitch angle,  $\theta$ , consists of collective ( $\theta_0$ ), two cyclic ( $\theta_c, \theta_s$ ), and blade twist ( $\theta_{tw}$ ) and it is

$$\theta = \theta_0 + \theta_c \cos(\psi) + \theta_s \sin(\psi) + \theta_{tw} (r/R) \quad (6)$$

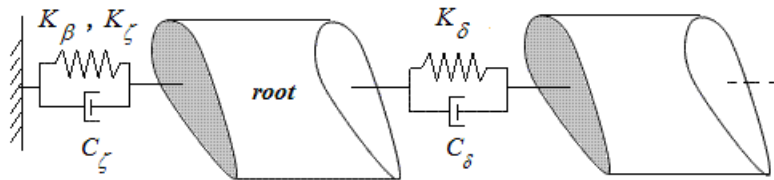
Here  $\psi$  is the blade azimuth angle. Assuming  $dL \gg dD$  ( $U_P/U_T$ ) (Leishman, 2006), the infinitesimal aerodynamic force and moment in lead-lagging and flapping frame are

$$d_{LLF} F_{aero} = \begin{bmatrix} 0 & -dL (U_P/U_T) & -dD & dL \end{bmatrix}^T, \quad d_{LLF} M_{aero} = \begin{bmatrix} 0 & -r dL & r (-dL (U_P/U_T) - dD) \end{bmatrix}^T \quad (7)$$

### Blade flexibility

Lumped system modeling is used for blade flexibility. Flapwise bending is considered. The blades are divided into rigid segments joined by flapwise bending springs and dampers as illustrated in Figure 3.

**Figure 3** Lumped System Modeling



The flapping angle of the  $(i+1)$ -th blade segment is

$${}_{i+1}\beta = \beta + \sum_{k=1}^i \delta_k, \quad i = 1, \dots, n-1 \quad (8)$$

where  $n$  is the number of blade segments,  $C_\zeta$  is the damping coefficient of lead-lagging damper,  $\delta_k$  is the deflection angle of the  $k$ -th flapwise bending spring,  ${}_{i+1}\beta$  is the flapping angle of the  $(i+1)$ -th blade segment, and  $\beta$  is the root flapping angle. The blades are divided into three segments.

### Multi blade equations

Each blade motion is assumed synchronous (Padfield, 2007). Ignoring higher harmonic terms and using 4 blades for the main rotor, blade flapping, lead-lagging and flapwise bending motions are described by

$$\Theta_i = \Theta_0 + \Theta_c \cos(\psi_i) + \Theta_s \sin(\psi_i) + \Theta_d (-1)^i \quad \& \quad \psi_i = \psi - (\pi/2)(i-1), \quad i = 1, \dots, 4 \quad (9)$$

Here  $\Theta$  is the generic notation for any of the three angles mentioned above, while  $\Theta_0$ ,  $\Theta_c$ ,  $\Theta_s$ , and  $\Theta_d$  are collective, two cyclic and differential components respectively.

### Main rotor downwash

The downwash is linearly distributed along the blade and its cyclic components,  $\lambda_c$ ,  $\lambda_s$ , are (Leishman, 2006, Pitt and Peters model)

$$\lambda_c = \lambda_0 \frac{15\pi}{23} \tan\left(\frac{\chi}{2}\right), \quad \lambda_s = 0, \quad \chi = \tan^{-1}\left(\frac{u}{w + \lambda_0}\right) \quad (10)$$

where  $\chi$  is the wake skew angle. The uniform component of the downwash,  $\lambda_0$ , can be calculated numerically using momentum theory:

$$\frac{T}{2\rho\pi R^2} = \lambda_0 \sqrt{u^2 + v^2 + (\lambda_0 - w)^2} \quad (11)$$

where  $u$ ,  $v$ ,  $w$  are helicopter linear velocity components in aircraft frame,  $\rho$  is the air density, and  $T$  is the main rotor thrust.

### Fuselage model

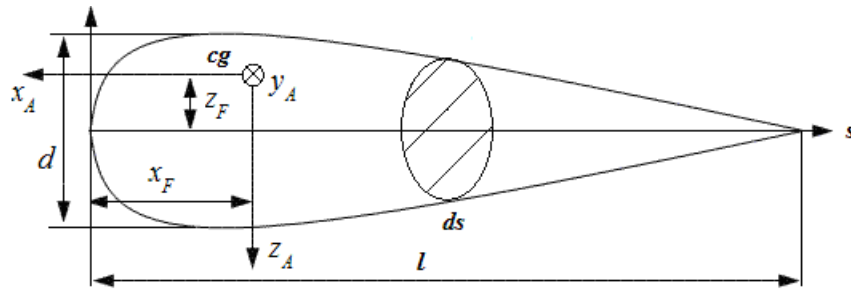
For our models an analytic formulation (Drela, 1999), derived using slender body theory, is preferred for fuselage modeling. For a body of revolution (Figure 4), the infinitesimal aerodynamic forces and moments acting on a fuselage strip of length  $ds$  are

$$d\vec{f}_{Lift} = \rho \vec{V}_\perp V_1 2\pi R_f(s) \frac{d}{ds} R_f(s) ds, \quad d\vec{M}_{Lift} = \vec{r}_{AS} \otimes d\vec{f}_{Lift}$$

$$d\vec{f}_{Drag} = \frac{1}{2} \rho |\vec{V}| \vec{V} 2R_f(s) c_{d_f} ds + \frac{1}{2} \rho |\vec{V}_\perp| \vec{V}_\perp 2R_f(s) c_{d_p} ds, \quad d\vec{M}_{Drag} = \vec{r}_{AS} \otimes d\vec{f}_{Drag} \quad (12)$$

where  $R_f(s)$  is the fuselage radius at distance  $s$  along the fuselage reference line (FRL) measured from the nose,  $\vec{r}_{AS}$  is the position vector of  $s$ ,  $\vec{V}$  is the local air velocity,  $\vec{V}_\perp$  and  $V_1$  are local air velocity's components perpendicular and parallel to FRL respectively.

**Figure 4** Fuselage Subsystem



The pressure drag,  $c_{d_p}$ , and skin friction drag,  $c_{d_f}$ , are estimated from Hoerner, 1965. The profile function of the fuselage radius is

$$R_f(s) = 2d \left( \sqrt{\frac{s}{l}} - \frac{s}{l} \right) \quad (13)$$

where  $l$  and  $d$  are fuselage length and height, respectively (Figure 4,  $x_F, z_F$  are horizontal and vertical distances from  $cg$  to fuselage nose and  $x_A, y_A, z_A$  are unit vectors of aircraft frame). Assuming that the fuselage is in uniform downwash,  $\vec{V}$  is

$$\vec{V} = - {}^I \vec{V}_S + {}^I \vec{V}_{\lambda_0} \quad (14)$$

with the kinematic velocity at distance  $s$  on the FRL and the uniform downwash (in aircraft frame)

$${}^I \vec{V}_S = {}^I \vec{V}_A + {}^I \vec{\omega}^A \otimes \vec{r}_{AS}, \quad {}^I V_{\lambda_0} = [0 \quad 0 \quad \lambda_0]^T \quad (15)$$

where  $\vec{r}_{AS}$  in aircraft frame is  ${}^A r_{AS} = [x_F - s \quad 0 \quad z_F]^T$ ,  ${}^I \vec{V}_A$  and  ${}^I \vec{\omega}^A$  are absolute helicopter linear and angular velocities.

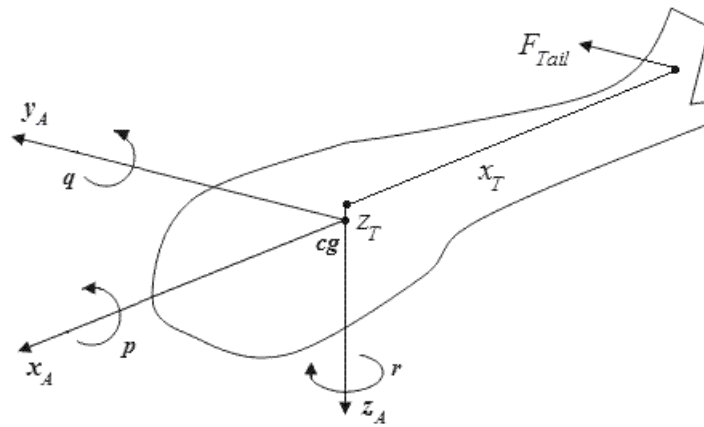
Integrating the infinitesimal aerodynamic forces and moments along the fuselage span, the fuselage aerodynamic force and moment are obtained.

### Tail rotor model

The tail rotor does not flap, is not canted, creates a force in anti-torque direction, its induced inflow is ignored, and its thrust in aircraft frame is

$${}^A F_{Tail} = [0 \quad K_T \theta_T \quad 0]^T \quad (16)$$

**Figure 5** Tail Rotor Subsystem



where  $x_T, z_T$  are horizontal and vertical distances from cg to tail rotor,  $K_T$  is the maximum thrust coefficient, chosen to keep the collective pitch angle of tail  $\theta_T \leq 1$  rad. In Figure 5 the tail rotor subsystem is illustrated. The tail rotor moment around cg is

$$\vec{M}_{Tail} = \vec{r}_T \otimes \vec{F}_{Tail} \quad (17)$$

where tail rotor position w.r.t. cg in aircraft frame is

$${}^A r_T = [-x_T \quad 0 \quad -z_T]^T \quad (18)$$

The tail rotor hub and shaft drag force and moment are

$$\vec{D}_{h\&s} = \frac{1}{2} \rho \left| {}^I \vec{V}_T \right| {}^I \vec{V}_T S_{h\&s} c_{d_{h\&s}}, \quad \vec{M}_{h\&s} = \vec{r}_T \otimes \vec{D}_{h\&s} \quad (19)$$



where the frontal area and drag coefficient of the tail rotor hub and shaft,  $S_{h\&s}$  and  $c_{d_{h\&s}}$ , are estimated from Prouty, 2005, while local air velocity of the tail rotor is

$${}^I\vec{V}_T = -\left({}^I\vec{V}_A + {}^I\vec{\omega}^A \otimes \vec{r}_T\right) \quad (20)$$

### Model simplification

At the end of this modeling process, implemented using Maple, we find the nonlinear equations of motion in implicit form:

$$f(\dot{x}, x, v) = 0 \quad (21)$$

where  $f \in \mathbb{R}^{44}$ ,  $x \in \mathbb{R}^{41}$ , and  $v \in \mathbb{R}^4$  ( $x$  and  $v$  are nonlinear state and control vectors). Note that the discrepancy between the size of  $f(44)$  and the size of  $x(41)$  is due to the three static downwash equations.

The number of terms in Equation 21 is huge (of the order  $10^5$ ). To reduce this number an ordering scheme (see Oktay, 2012 and Schwarz, 2009) is applied. The idea is to neglect terms whose relative magnitude w.r.t. the largest term in an expression is smaller than a specific amount. To apply the ordering scheme to the dynamic equations, each term is assigned an order of magnitude based on physical considerations. For example the trim value of  $\beta$  is 3–6 degrees (Leishman, 2006) and the trim value of  $\zeta$  is small (Leishman, 2006). The trim values of collective flapping and lead-lagging angles ( $\beta_0$  and  $\zeta_0$ ) are generally larger than cyclic angles ( $\beta_c, \beta_s, \zeta_c, \zeta_s$ ). The trim values of differential angles ( $\beta_d$  and  $\zeta_d$ ) are zero. Therefore, the orders are chosen as

$$|\beta_0| = |\zeta_0| = 0.2 \text{ rad}, \quad |\beta_c| = |\beta_s| = |\zeta_c| = |\zeta_s| = 0.1 \text{ rad}, \quad |\beta_d| = |\zeta_d| = 0.1 \text{ rad} \quad (22)$$

The orders of  $u, v, w$  are determined by ignoring  $p, q, r$  (helicopter angular velocities in aircraft frame). For many helicopters (e.g. Puma SA 330, Bo 105) the maximum forward speed is around 70 m/s. Therefore, the order of  $u$  is chosen as 70 m/s. Because of drag limitation, the order of  $v$  is chosen as 35 m/s. Since  $w$  is generally smaller than 12 m/s, the order of  $w$  is chosen as 12 m/s. The bounds of main rotor control inputs are given in Prouty, 2005. The maximum  $\theta_0$  and  $\theta_c$  are around 20 degrees. Since  $\theta_c$  takes negative and positive values and  $\theta_s$  has same order with  $\theta_c$ , we choose their orders as

$$|\theta_0| = 0.35 \text{ rad}, \quad |\theta_c| = 0.175 \text{ rad}, \quad |\theta_s| = 0.175 \text{ rad} \quad (23)$$

## Trim, Linearization, Model Validation

Here trim is the condition for which straight level flight with constant speed ( $V_A$ ) is achieved. **Note that we refer to all flights for which  $V_A \leq 1$  kt as “hover” because of the very small value of  $V_A$ .** We obtained 25 trim equations (3 force and 3 moment helicopter equations, 8 flapping and lead-lagging equations, 8 flapwise bending equations, and 3 main rotor downwash equations) and 25 unknowns. The trim values of helicopter angular velocities and yaw angle ( $\psi_A$ ) are zero. The helicopter linear velocities are function of  $V_A$ , roll ( $\phi_A$ ) and pitch ( $\theta_A$ ) angles of helicopter. The vector of trim unknowns is

$$x_0 = [\underbrace{\theta_{0_0}, \theta_{c_0}, \theta_{s_0}, \theta_{T_0}}_{controls}, \underbrace{\phi_{A_0}, \theta_{A_0}}_{Euler}, \underbrace{\beta_{0_0}, \beta_{c_0}, \beta_{s_0}, \beta_{d_0}}_{flapping}, \underbrace{{}_2\beta_{0_0}, {}_2\beta_{c_0}, {}_2\beta_{s_0}, {}_2\beta_{d_0}, {}_3\beta_{0_0}, {}_3\beta_{c_0}, {}_3\beta_{s_0}, {}_3\beta_{d_0}}_{flapwise bending}, \underbrace{\zeta_{0_0}, \zeta_{c_0}, \zeta_{s_0}, \zeta_{d_0}}_{lead-lagging}, \underbrace{\chi_0, \lambda_{0_0}, \lambda_{c_0}}_{downwash}]^T \quad (24)$$

Matlab's fsolve was used to solve the trim equations for hover and different flight speeds. The results were verified by inserting them into the dynamic equations obtained after ordering scheme application. Small numbers (around  $10^{-10}$ ) were obtained showing that trimming is correct. For hover and  $V_A = 80$  kts, the trims are

$$\begin{aligned} \text{hover } x_0 &= [ \underbrace{0.2686, 0.0094, -0.0255, 0.0952}_{\theta_{0_0}, \theta_{c_0}, \theta_{s_0}, \theta_{T_0}}, \underbrace{-0.0057, 0.0238}_{\phi_{A_0}, \theta_{A_0}}, \underbrace{0.0472, 0.0230, 0.0021, 0}_{\beta_{0_0}, \beta_{c_0}, \beta_{s_0}, \beta_{d_0}}, \underbrace{0.0681, 0.0283, 0.0032, 0}_{{}_2\beta_{0_0}, {}_2\beta_{c_0}, {}_2\beta_{s_0}, {}_2\beta_{d_0}}, \\ &\quad \underbrace{0.0855, 0.0319, 0.0045, 0}_{{}_3\beta_{0_0}, {}_3\beta_{c_0}, {}_3\beta_{s_0}, {}_3\beta_{d_0}}, \underbrace{0.0172, -0.0009, -0.0027, 0}_{\zeta_{0_0}, \zeta_{c_0}, \zeta_{s_0}, \zeta_{d_0}}, \underbrace{0.0237, 11.2975, 0.2835}_{\chi_0, \lambda_{0_0}, \lambda_{c_0}} ]^T \\ \text{80kts } x_0 &= [ \underbrace{0.2493, 0.0243, -0.1147, 0.0594}_{\theta_{0_0}, \theta_{c_0}, \theta_{s_0}, \theta_{T_0}}, \underbrace{-0.0035, 0.0312}_{\phi_{A_0}, \theta_{A_0}}, \underbrace{0.0524, 0.0327, -0.0005, 0}_{\beta_{0_0}, \beta_{c_0}, \beta_{s_0}, \beta_{d_0}}, \underbrace{0.0660, 0.0432, -0.0097, 0}_{{}_2\beta_{0_0}, {}_2\beta_{c_0}, {}_2\beta_{s_0}, {}_2\beta_{d_0}}, \\ &\quad \underbrace{0.0729, 0.0553, -0.0276, 0}_{{}_3\beta_{0_0}, {}_3\beta_{c_0}, {}_3\beta_{s_0}, {}_3\beta_{d_0}}, \underbrace{0.0123, -0.0048, -0.0048, 0}_{\zeta_{0_0}, \zeta_{c_0}, \zeta_{s_0}, \zeta_{d_0}}, \underbrace{1.4617, 3.2805, 6.0345}_{\chi_0, \lambda_{0_0}, \lambda_{c_0}} ]^T \end{aligned} \quad (25)$$

where all trim angles are given in radians and  $\lambda_{0_0}, \lambda_{c_0}$  are in m/s. After trimming, our model was linearized using Maple, **yielding continuous linear time-invariant systems**

$$\dot{x}_p = A_p x_p + B_p u \quad (26)$$

where  $x_p$  and  $u$  are the perturbed states and control inputs. Matrices  $A_p$  and  $B_p$  are of size  $41 \times 41$  and  $41 \times 4$ . There are 9 fuselage and 32 main rotor states, 3 main rotor and 1 tail rotor controls.

Puma SA 330 was used to validate the models previously developed with most technical data taken from Padfield, 2007. We ascertained good match with results in the literature for many flight conditions. For example, most flight

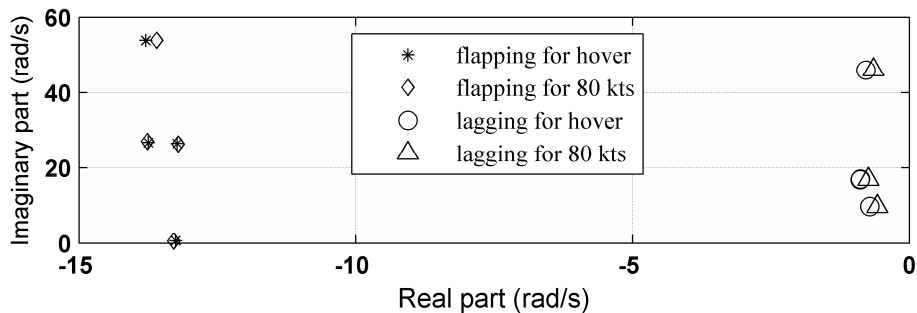
dynamics modes (linearized system eigenvalues) of our model for hover and  $V_A = 80\text{kts}$ , shown in Table 1, match well results reported in Padfield, 2007. The 4<sup>th</sup> mode does not match well due to modeling discrepancy between our model and Padfield, 2007, however, the qualitative behavior is similar (exponentially stable mode). The matrices  $A_p$  and  $B_p$  of the linearized model around hover and  $V_A = 40\text{kts}$  are provided in the Appendix.

**Table 1** Flight Dynamic Modes Comparison.

MODE (rad/s)	HOVER		80 KTS	
	OUR MODEL	PADFIELD	OUR MODEL	PADFIELD
1 <sup>st</sup> mode	$0.1753 \pm 0.5816i$	$0.2772 \pm 0.5008i$	$-0.5294 \pm 2.5879i$	$-0.1854 \pm 1.0546i$
2 <sup>nd</sup> mode	$0.0779 \pm 0.4357i$	$-0.0410 \pm 0.5691i$	$-0.0166 \pm 0.1572i$	$-0.0085 \pm 0.2074i$
3 <sup>rd</sup> mode	-0.1514	-0.2697	-0.02752	-0.1358
4 <sup>th</sup> mode	-1.1540	-0.3262	-1.0737	-1.5163
5 <sup>th</sup> mode	$-0.9987 \pm 0.3405i$	$-1.2990 \pm 0.2020i$	$-1.1014 \pm 2.2242i$	$-0.9252 \pm 1.0503i$

The qualitative behavior of our flapping and lead-lagging modes is identical with the one described in Padfield, 2007. For example, the flapping modes are much farther away from the imaginary axis compared to the lagging modes and the magnitude of the frequency bound for the flapping modes is larger than the one for the lagging modes (Figure 6). All trim results also showed good correspondence with data in the literature (see the references in model simplification sub-section).

**Figure 6** Flapping and Lead-Lagging Modes



## Constrained MPC

MPC has emerged as one of the best technologies to handle multiple, simultaneous and even discontinuous constraints on states and controls. MPC is also increasingly used in practice because it relies on models for predicting the system behavior and it has the potential for online adaptation (Maciejowski, 2001; Camacho and Bordons, 1999; Mayne et al., 2000). Therefore, we design MPC controllers and also investigate MPC's robustness. A brief description of MPC is given next.

In constrained MPC, a cost function  $V(k)$  :

$$V(k) = \sum_{i=1}^{H_p} \left\| \hat{y}(k+i|k) - r(k+i|k) \right\|_{Q(i)}^2 + \sum_{i=0}^{H_u-1} \left\| \Delta \hat{u}(k+i|k) \right\|_{R(i)}^2 \quad (27)$$

is minimized subject to the discretized dynamic equations and some constraints:

$$E \begin{bmatrix} \Delta U(k) \\ \mathbf{1} \end{bmatrix} \leq 0; \quad F \begin{bmatrix} U(k) \\ \mathbf{1} \end{bmatrix} \leq 0; \quad G \begin{bmatrix} Y(k) \\ \mathbf{1} \end{bmatrix} \leq 0 \quad (28)$$

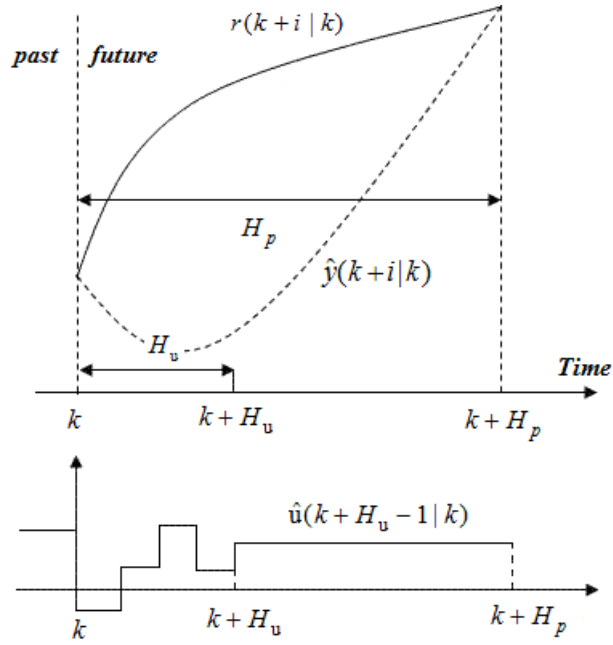
where

$$\Delta U(k) = \begin{bmatrix} \Delta \hat{u}_1(k|k) & \cdot & \Delta \hat{u}_1(k+H_u-1|k) \\ \cdot & \cdot & \cdot \\ \Delta \hat{u}_{n_u}(k|k) & \cdot & \Delta \hat{u}_{n_u}(k+H_u-1|k) \end{bmatrix}, \quad U(k) = \begin{bmatrix} \hat{u}_1(k|k) & \cdot & \hat{u}_1(k+H_u-1|k) \\ \cdot & \cdot & \cdot \\ \hat{u}_{n_u}(k|k) & \cdot & \hat{u}_{n_u}(k+H_u-1|k) \end{bmatrix}$$

$$Y(k) = \begin{bmatrix} \hat{y}_1(k+1|k) & \cdot & \hat{y}_1(k+H_p|k) \\ \cdot & \cdot & \cdot \\ \hat{y}_{n_y}(k+1|k) & \cdot & \hat{y}_{n_y}(k+H_p|k) \end{bmatrix} \quad (29)$$

$E$ ,  $F$ , and  $G$  are suitable matrices,  $n_y$  and  $n_u$  are the number of outputs and inputs,  $H_p$  and  $H_u$  are prediction and control horizons,  $Q(i)$  and  $R(i)$  are matrix weights used in the corresponding Euclidean norms computation and they were taken as identity matrices in this paper,  $\hat{y}(k+i|k)$  is the predicted output,  $\hat{u}(k+i|k)$  and  $\Delta \hat{u}(k+i|k)$  are the predicted input and predicted input variation, and  $r(k+i|k)$  is the reference trajectory to be tracked (Figure 7). The optimization problem in Equations 27-29 is equivalent to a quadratic programming problem (Maciejowski, 2001). After solving it, only the first control in the resulting optimal control policy is applied and the optimization control problem is repeated for the next time horizon.

**Figure 7** MPC Representation



Our main goal is to investigate the ability of MPC to track discontinuous trajectories while obeying heterogeneous constraints. Furthermore, we want to evaluate the possibility of reliably using MPC with our sophisticated models. For this purpose we analyzed MPC design using our linearized models, which were discretized using a nondimensionalized sampling time of 1 rad (0.037s). **The plant and measurements were assumed to be corrupted by additive Gaussian white noise. This means that the plant dynamics equation, Equation 26, becomes  $\dot{x}_p = A_p x_p + B_p u + w_p$  where  $w_p$  is the plant noise and the measurement equation is  $z = M_p x_p + v$  where  $M_p$  is the measurement matrix and  $v$  is the measurement noise. The measurements were 9 fuselage states (helicopter linear and angular velocities and Euler angles) so using Matlab,  $M_p = [\text{eye}(9), \text{zeros}(9,32)]$ .**

In the first example, the model linearized around hover and given in the Appendix was used. The helicopter is required to track a reference trajectory for which the roll angle has a prescribed time variation and the other two Euler angles are forced to be zero. The parameters used for 1<sup>st</sup> MPC design were

$$\begin{bmatrix} -1 \\ -0.01 \\ -0.01 \end{bmatrix} \leq \begin{bmatrix} \phi_A \\ \theta_A \\ \psi_A \end{bmatrix} (\text{rad}) \leq \begin{bmatrix} 0 \\ 0.01 \\ 0.01 \end{bmatrix}; \begin{bmatrix} |p| \\ |q| \\ |r| \end{bmatrix} (\text{rad/s}) \leq \begin{bmatrix} 1 \\ 1 \\ 1 \end{bmatrix}; \begin{bmatrix} 0 \\ -0.18 \\ -0.18 \\ 0 \end{bmatrix} \leq \begin{bmatrix} \theta_0 \\ \theta_c \\ \theta_s \\ \theta_T \end{bmatrix} (\text{rad}) \leq \begin{bmatrix} 0.35 \\ 0.18 \\ 0.18 \\ 1 \end{bmatrix}; \begin{bmatrix} \Delta\theta_0 \\ \Delta\theta_c \\ \Delta\theta_s \\ \Delta\theta_T \end{bmatrix} (\text{rad}) \leq \begin{bmatrix} 0.175 \\ 0.09 \\ 0.09 \\ 0.5 \end{bmatrix}; H_p = 20; H_u = 2 \quad (30)$$

For the second example, previous linearized model was used. The helicopter is required to track a reference trajectory for which helicopter pitch angle has a prescribed time variation and the other two Euler angles are forced to be zero. The parameters used for 2<sup>nd</sup> MPC design are the same with first example except that

$$[-0.01 \quad -1 \quad -0.01]^T \leq [\phi_A \quad \theta_A \quad \psi_A]^T \text{ (rad)} \leq [0.01 \quad 0 \quad 0.01]^T \quad (31)$$

In the third example, to evaluate the robustness of our MPC designs we considered that *all* helicopter inertial parameters (helicopter mass and helicopter inertia matrix elements) are uncertain. For this purpose we considered that the plant model's inertial parameters decrease by 10%, while the internal model, which is used to produce MPC signals, is not aware of these uncertainties. We then simulated the response of the plant affected by these uncertainties. The linearized model, trajectories and parameters used for MPC design are the same with the first example.

For the fourth example, the helicopter model was linearized around straight level flight at 40kts. The trajectory and other MPC parameters are the same with the first example, but the simulation time is 3.7s.

For the fifth example, robustness of previous MPC w.r.t. variation of helicopter inertial parameters is examined. For this purpose we considered that the plant model's inertial parameters decrease by 10%, while the internal model is not aware of these uncertainties. The only difference from the fourth example is that

$$[-1 \quad -0.02 \quad -0.02]^T \leq [\phi_A \quad \theta_A \quad \psi_A]^T \text{ (rad)} \leq [0 \quad 0.02 \quad 0.02]^T \quad (32)$$

To show the feasibility of MPC for other flight conditions we used a model linearized around a helical turn ( $V_A = 40$  kts, the turn rate is 0.1rad/s, and the flight path angle is 0.1rad; see Oktay, 2012 for details) for the sixth example. The helicopter is required to track a reference trajectory for which the roll angle has a prescribed time variation and the other two Euler angles are forced to be zero. The simulation time is 3.7s. MPC parameters are same with first example except that

$$H_u = 1, \quad [-1 \quad -0.02 \quad -0.02]^T \leq [\phi_A \quad \theta_A \quad \psi_A]^T \text{ (rad)} \leq [1 \quad 0.02 \quad 0.02]^T \quad (33)$$

Note that the closed loop responses are variations from the trim values and Matlab was used for simulations.

**Figure 8** Selected Closed Loop Responses Using 1<sup>st</sup> MPC

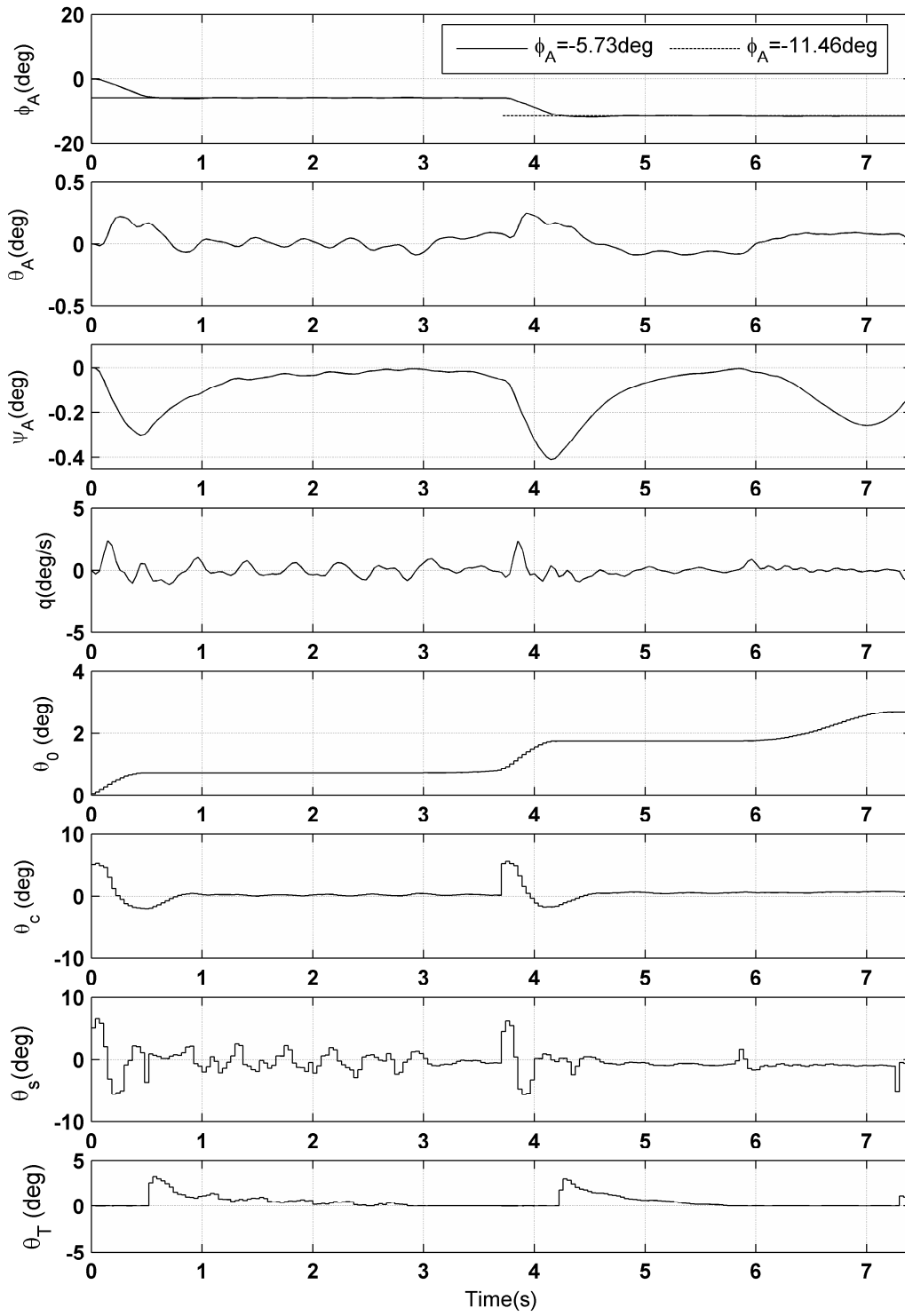


**Figure 9** Selected Closed Loop Responses Using 2<sup>nd</sup> MPC

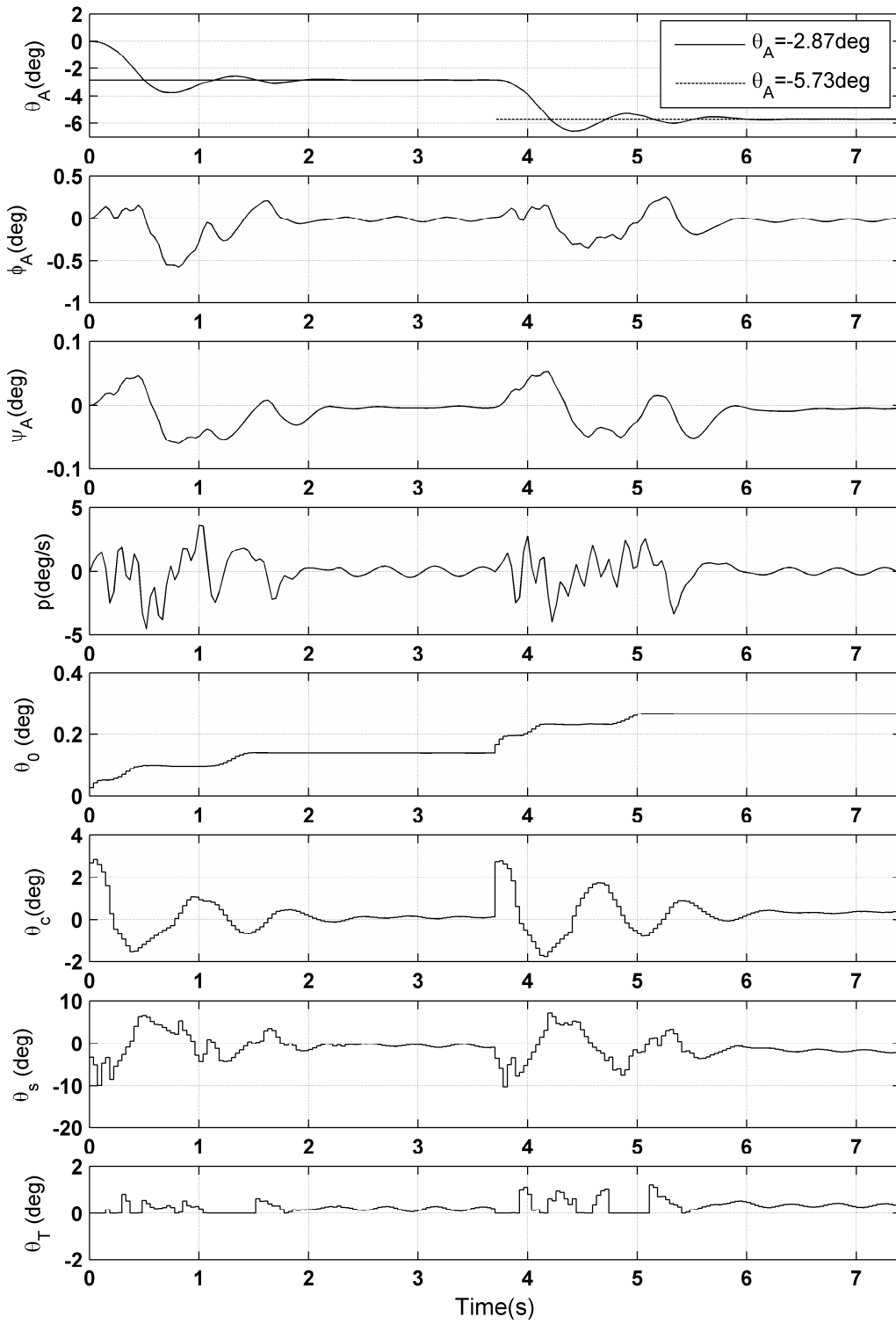




Figure 10 Selected Closed Loop Responses Using 3<sup>rd</sup> MPC

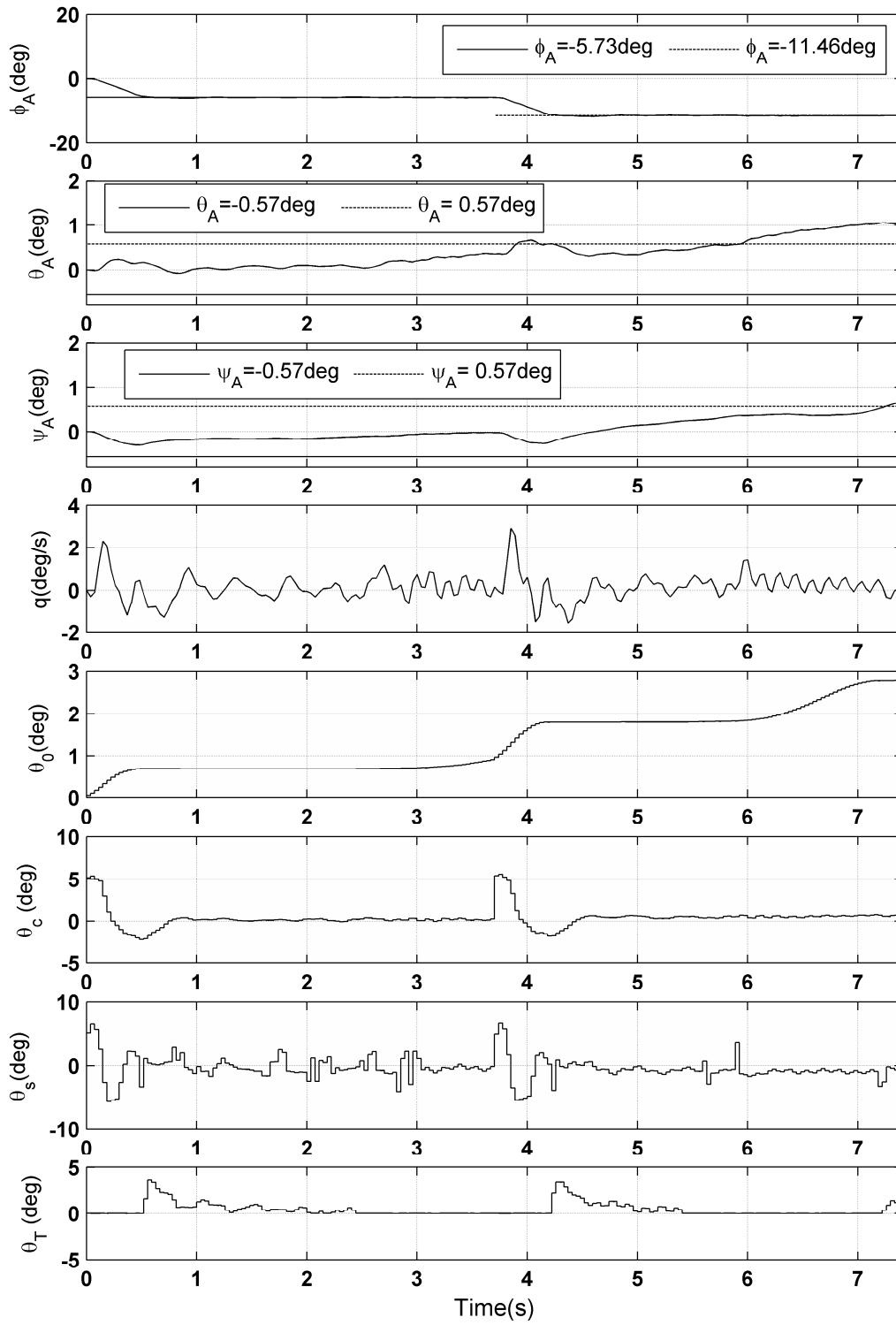


Figure 11 Selected Closed Loop Responses Using 4<sup>th</sup> MPC

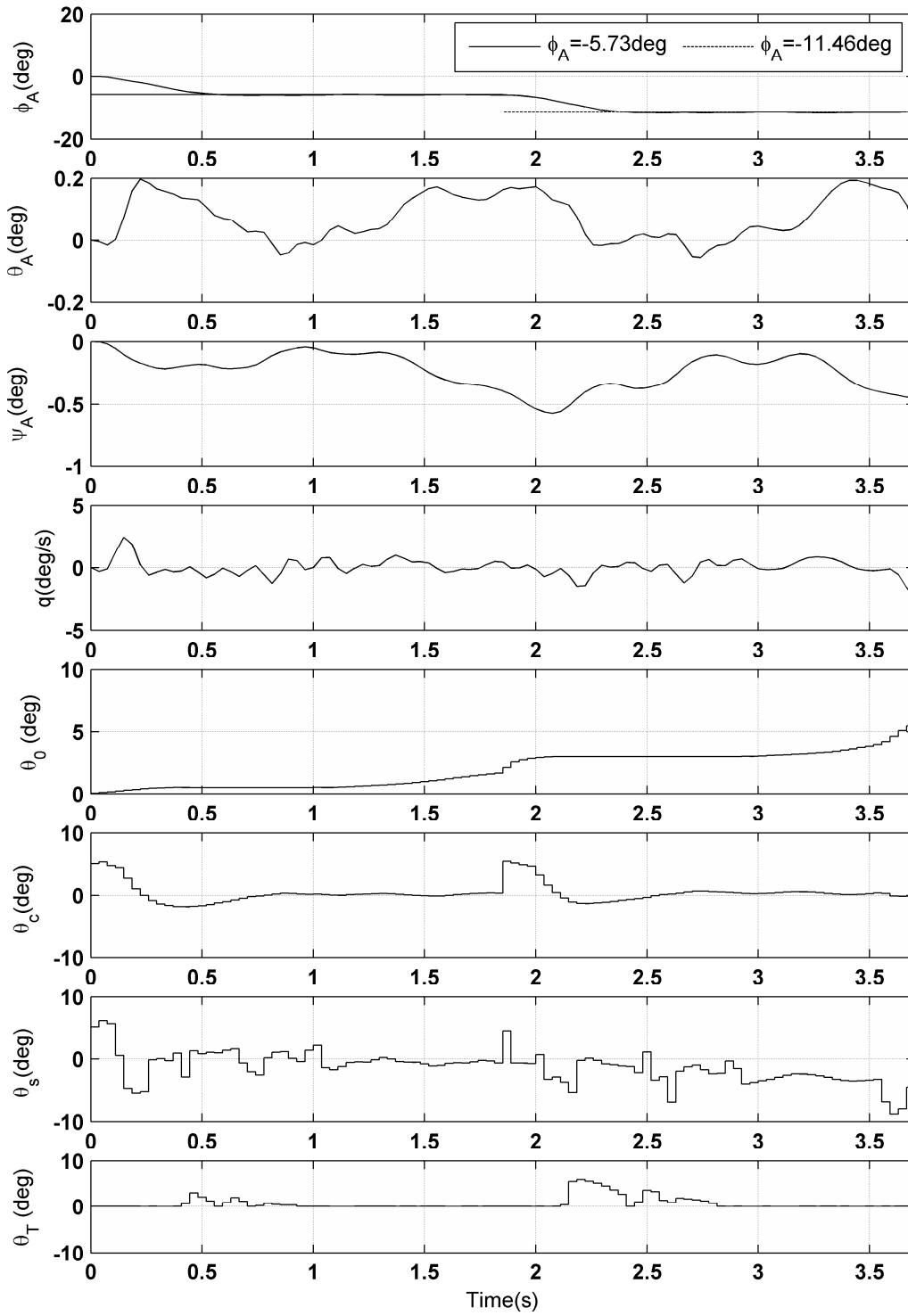


Figure 12 Selected Closed Loop Responses Using 5<sup>th</sup> MPC

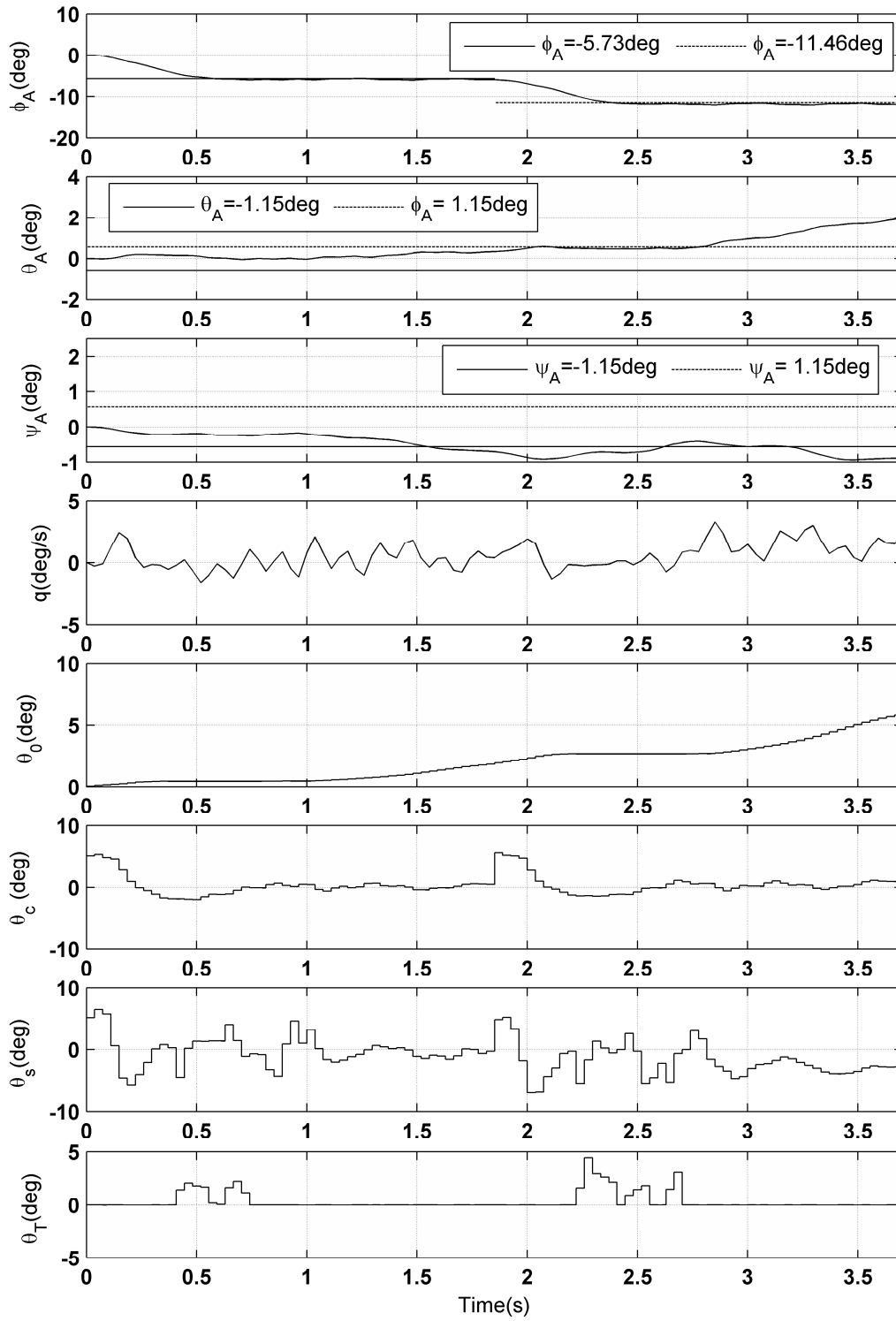
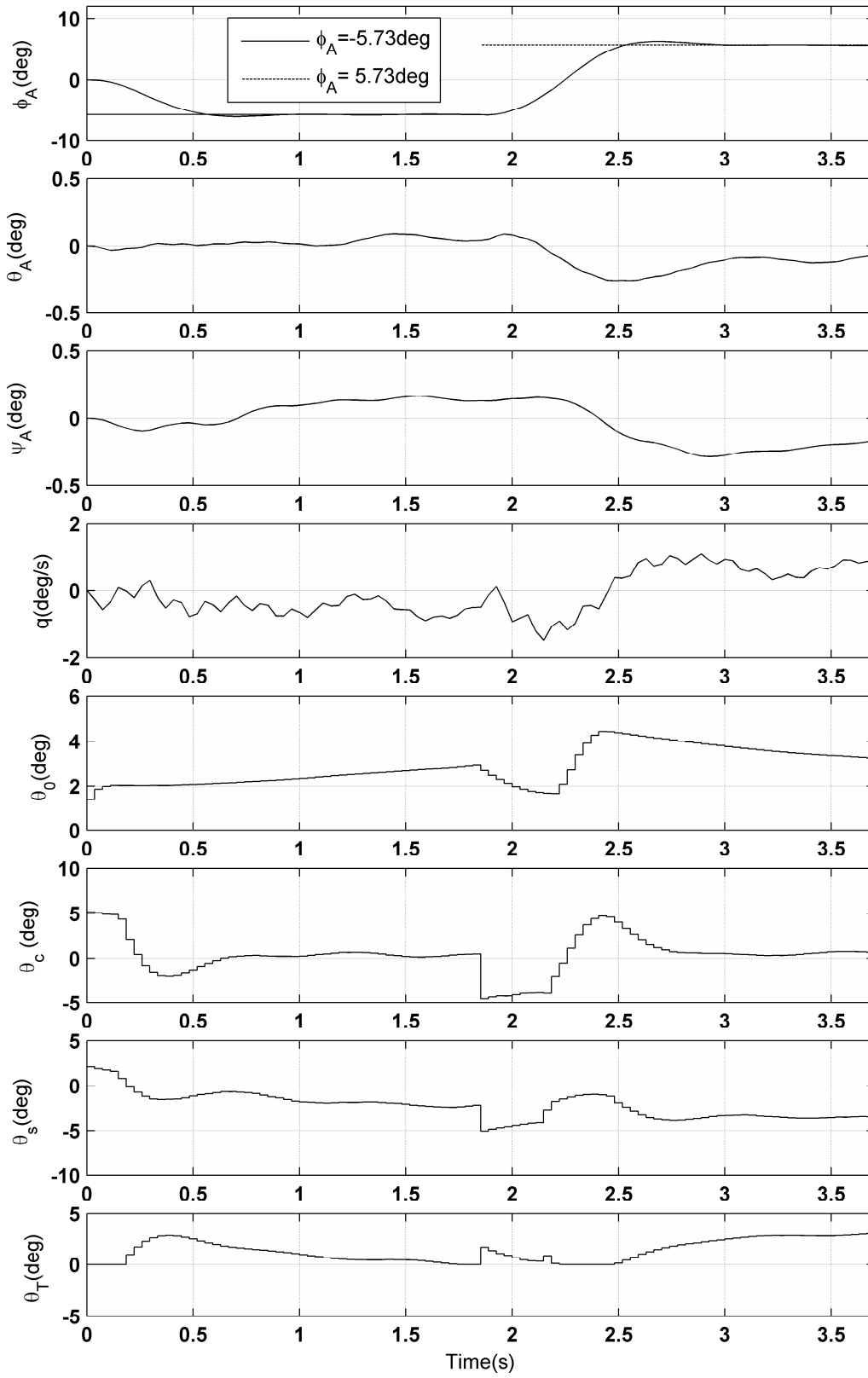


Figure 13 Selected Closed Loop Responses Using 6<sup>th</sup> MPC



Calculation times of our MPCs are less than 0.2 radians (0.0074 s) which is 20% of the sampling time. Importantly, in all our nominal designs (when the plant is not affected by modeling uncertainties) MPC satisfied the constraints (see Figures 8,9,11,13). When modeling uncertainties (variation of inertial parameters) were considered, some of the plant outputs (helicopter pitch and yaw angles) violated the constraints (see Figures 10 and 12). These violations are larger in the fifth example than in the third. However, none of these violations is extreme.

It is also remarked that good tracking was achieved for *all* examples even when modeling uncertainties were considered. Our extensive simulations show that the other states ( $u, v, w, p, q, r$ ) which are not included in the reference trajectory tracked by our MPC do not experience catastrophic behavior (e.g. large and fast variations).

Finally, our extensive experiments show that MPC is also successful in tracking different, highly constrained trajectories for many other straight level flights and helical turns, and also banked turns (see Oktay, 2012).

## Conclusions

Control oriented helicopter models are derived using physics principles. Validation of the models used for control against data from the literature indicates that our modeling process correctly captures essential helicopter dynamics, including flight dynamics, flapping, lead-lagging modes and trims. These models are used for advanced constrained control design, namely model predictive control (MPC). Our studies show that tracking of highly constrained discontinuous trajectories for sophisticated helicopter models using MPC is feasible. MPC is also robust to modeling uncertainties (i.e. variation of all helicopter inertial quantities).

## References

- Afonso, R. J. M. and Galvao, R. K. H. (2010), "Predictive Control of a Helicopter Model with Tolerance to Actuator Faults", *IEEE Control and Fault Tolerant Systems Conference*, Nice, France.
- Bogdanov, A. A. and Wan, E. A. (2001), "Model Predictive Neural Control of a High-Fidelity Helicopter Model", *AIAA Guidance Navigation and Control Conference*, Montreal, Canada.
- Bottasso, C. L. and Riviello, L. (2005), "Rotor Trim by a Neural Model-Predictive Auto-Pilot", *Proceedings of the 32nd European Rotorcraft Forum*, Florence, Italy.
- Camacho, E. F. and Bordons, C. (1999), *Model Predictive Control*, Springer, pp. 167-205.
- Dalamagkidis, K., Valavanis, K. P., and Piegl, L. A (2010)., "Nonlinear Model Predictive Control with Neural Network Optimization for Autonomous Autorotation of Small Unmanned Helicopters", *IEEE Transactions on Control Systems Technology*, Vol. 19, no. 4, pp. 1-14.
- Drela, M. (1999), "Integrated Simulation Model for Preliminary Aerodynamic, Structural, and Control-Law Design of Aircraft", *40th Structures, Structural Dynamics and Materials Conference*, Saint Louis, MO, USA.
- Dreier, M. E. (2007), *Introduction to Helicopter and Tiltrotor Flight Simulation*, AIAA Education Series, p. 591.
- Done, G. and Balmford, D. (2001), *Bramwell's Helicopter Dynamics*, Second Edition, AIAA Press, pp. 21-23.

Dutka, A. S., Ordys, A. W., and Grimble, M. J. (2003), "Non-linear Predictive Control of 2 DOF Helicopter Model", *42nd IEEE Conference on Decision and Control*, Maui, HI, USA.

Hodges, D. H. and Dowell, E. H. (1974), "Nonlinear Equations of Motion for the Elastic Bending and Torsion of the Twisted Nonuniform Rotor Blades", NASA TN D-7818.

Hoerner, S. F. (1965), *Fluid Dynamic Drag*, Hoerner Fluid Dynamics, pp. 2.1, 3.9.

Joelianto, E., Sumarjono, E. M., Budiyo, A., and Retnaning, D. (2011), "Model Predictive Control For Autonomous Unmanned Helicopters", *Aircraft Engineering and Aerospace Technology*, Vol. 83, no. 6, pp. 375-387.

Leishman, J. G. (2006), *Principles of Helicopter Aerodynamics*, Third Edition, Cambridge University Press, pp. 118, 160, 174, 195.

Maciejowski, J. M. (2001), *Predictive Control with Constraints*, Prentice Hall, Pearson Education, pp. 74-83.

Mayne, D. Q., Rawlings, J. B., Rao, C. V., and Sokaert, P. O. M. (2000), "Constrained Model Predictive Control: Stability and Optimality", *Automatica*, Vol. 36, no. 6, pp. 789-814.

Oktay, T. (2012), "Constrained Control of Complex Helicopter Models", *Ph.D. Dissertation*, Virginia Tech, USA, May 2012.

Padfield, G. D. (2007), *Helicopter Flight Dynamics*, Second Edition, AIAA Education Series, pp. 103, 137, 175-181, 282-287.

Phillips, W. H. (1948), "Effect of Steady Rolling on Longitudinal and Directional Stability", NACA TN 1627.

Prouty, R. W. (2005), *Helicopter Performance, Stability and Control*, Robert E. Kreiger Publishing Co., pp. 298, 299, 684-701.

Sahasrabudhe, V., Celi, R., and Tits, A. (1997), "Integrated Rotor-Flight Control System Optimization with Aeroelastic and Handling Qualities Constraints", *Journal of Guidance, Control, and Dynamics*, Vol. 20, no. 2, pp. 217-225.

Sahasrabudhe, V. and Celi, R. (1997), "Efficient Treatment of Moderate Amplitude Constraints for Handling Qualities Design Optimization", *Journal of Aircraft*, Vol. 34, no. 6, pp. 730-739.

Schwarz, J. L. R. (2009), "Ordering Scheme and Reduced Complexity Modeling for a Multi-Rigid Body Helicopter Dynamic Model", *MS Thesis*, TUM, Germany.

Traugott, J. P., Patil, M. J., and Holzappel, F. (2006), "Nonlinear Dynamics and Control of Integrally Actuated Helicopter Blades", *Aerospace Science and Technology*, Vol. 10, no. 6, pp. 509-518.

## Appendix

For hover flight and  $V_A = 40$  kts (i.e. straight level flight) the matrices of linearized models are given in Equations 34-38.

Matrix  $A_p$  can be obtained using  $A_p = [\xi, \Gamma]$ . The eigenvalues of  $A_p$  have to be multiplied by the main rotor angular speed,  $\Omega$  ( $\Omega = 27$  rad/s for Puma SA 330) to obtain dimensional modes of the helicopter. Note that the modes in Table 1 are in dimensional form. In Equations 34-38 the letter e represents  $10^e$ . In Equation 38 the perturbed state and control vectors are also given.

$1kt \xi =$

5.89e-5, 8.57e-5, 2.03e-5, -1.85e-3, 1.34e-4, -5.67e-9, 0, -1.79e-3, 0, 9.87e-6, -5.91e-5, -4.46e-4, -1.51e-4, -1.46e-4, -1.94e-4, -2.85e-7, -4.75e-7, -4.32e-5, -6.73e-5, 1.5e-4, 2.29e-2  
-7.64e-5, -1.51e-3, -1.91e-5, -6.2e-5, -1.77e-3, -9.59e-4, 1.79e-3, 2.43e-7, 0, 1.91e-5, -2.65e-4, -1.38e-4, -1.96e-4, 5.26e-4, 1.48e-4, -1.77e-6, -3.05e-6, -9.26e-5, 7.28e-6, 6.57e-3, -1.3e-5  
5.14e-5, -1.43e-5, -3.22e-3, 2.03e-4, 1.08e-3, -3.34e-8, 1.02e-5, -4.27e-5, 0, -4.4e-3, 3.44e-4, -4.27e-5, -1.31e-5, -8.43e-6, 1.68e-5, -3.89e-9, 9.72e-9, -4.69e-5, 3.44e-3, 2.22e-5, 6.8e-4  
-4.62e-4, 5.09e-3, -4.1e-4, 2.3e-3, -1.58e-2, -2.04e-3, 0, 0, 0, 2.41e-4, -2.6e-3, -1.56e-3, 6.28e-4, -1.46e-2, 8.22e-4, 1.86e-4, 6.29e-5, 5.98e-3, 3.18e-4, 6.45e-2, -2.94e-3  
6.39e-3, -2.86e-4, -7.49e-3, 4.83e-3, -2.53e-3, 5.51e-8, 0, 0, 0, -5.87e-5, -1.13e-004, -4.35e-3, 2.67e-4, 4.96e-4, -1.97e-4, -4.24e-5, 5.31e-5, 1.09e-4, 2.36e-4, -8.8e-4, -6.43e-2  
-4.71e-5, 5.44e-3, -3.53e-5, -3.23e-5, -2.69e-4, -5.19e-3, 0, 0, 0, 3.98e-5, -2.35e-4, -1.4e-4, 5.4e-5, -1.32e-3, 7.06e-5, 1.97e-5, 5.96e-6, 2.17e-2, 2.66e-3, 5.77e-3, -2.47e-4  
0, 0, 0, 1, -1.35e-4, 2.38e-2, 1.92e-18, 1.07e-17, 0, 0, 0, 0, 0, 0, 0, 0, 0, 0, 0, 0, 0, 0, 0, 0  
0, 0, 0, 0, 1, 5.69e-3, -1.07e-17, 0, 0, 0, 0, 0, 0, 0, 0, 0, 0, 0, 0, 0, 0, 0, 0, 0  
0, 0, 0, 0, -5.69e-3, 1, 8.09e-17, 2.54e-19, 0, 0, 0, 0, 0, 0, 0, 0, 0, 0, 0, 0, 0, 0, 0  
0, 0, 0, 0, 0, 0, 0, 0, 0, 0, 1, 0, 0, 0, 0, 0, 0, 0, 0, 0, 0  
-3.81e-2, 1.53e-2, 1.56, 5.78e-3, 1.82e-2, -3.39e-6, 0, 0, 0, -7.79, -9.3e-1, -2.94e-3, 4.69e-5, 3.7e-4, -1.08e-3, -2.63e-7, 8.21e-7, 2.1e-2, 4.02e-3, -7.2e-3, 1.86e-2  
0, 0, 0, 0, 0, 0, 0, 0, 0, 0, 0, 0, 1, 0, 0, 0, 0, 0, 0, 0, 0  
-7.25e-2, 3.22e-1, -4.19e-3, 2.01, 4.48e-1, 3.62e-5, 0, 0, 0, -7.91e-3, -7.36e-4, -6.79, -9.3e-1, -9.29e-1, -2, -4.82e-5, 5.53e-5, 1.01e-2, 3.89e-2, 1.89e-2, -6.54e-2  
0, 0, 0, 0, 0, 0, 0, 0, 0, 0, 0, 0, 0, 1, 0, 0, 0, 0, 0, 0, 0  
3.22e-1, 8.48e-2, 7.89e-3, 4.53e-1, -2.02, -2.16e-3, 0, 0, 0, 3.37e-4, -4.73e-3, 9.28e-1, 2, -6.8, -9.29e-1, 1.96e-4, 6.76e-5, 6.01e-3, 1.47e-2, 6.56e-2, -4.28e-3  
0, 0, 0, 0, 0, 0, 0, 0, 0, 0, 0, 0, 0, 1, 0, 0, 0, 0, 0, 0  
8.85e-24, 1.09e-23, 3.46e-23, 3.87e-24, 1.54e-24, -9.65e-28, 0, 0, 0, -1.22e-22, -3.6e-23, -2.5e-25, -7.34e-25, -5.73e-25, 2.26e-25, -7.79, -9.3e-1, -6.64e-22, -2.9e-21, -5.35e-26, -1.58e-24  
0, 1, 0, 0  
-6.57e-3, 2.5e-4, 6.13e-2, -1.65e-2, 2.45e-2, -2.51e-5, 0, 0, 0, -2.97e-4, -6.25e-2, -6.46e-3, -1.13e-2, 6.18e-4, 5.87e-3, 2.35e-6, 6.83e-7, -3.85e-1, -6.03e-2, -2.2e-3, 6.37e-5  
0, 1  
-5.97e-3, 4.69e-2, -7.57e-3, 8.35e-3, -3.87e-2, -1.18e-3, 0, 0, 0, -1.89e-3, -2.38e-2, -1.27e-4, -8.23e-2, -9.1e-2, 6.93e-4, 1.07e-4, 3.68e-5, 4.76e-6, -1e-3, 6.49e-1, -6.25e-2  
0, 0  
3.57e-2, 6.61e-3, -3.7e-2, -3.24e-2, -5.6e-3, -2.05e-5, 0, 0, 0, 2.45e-2, 1.13e-2, 8.51e-2, -3.58e-4, 3.86e-4, -8.25e-2, 2.63e-5, -3e-5, -2.52e-3, 6.76e-3, 6.16e-2, 2.04  
0, 0  
-8.56e-24, 1.12e-23, 8.75e-23, 3.17e-24, -4.04e-24, 1.01e-28, 0, 0, 0, -3.73e-23, 1.54e-21, 1.07e-24, 4.29e-24, 4.29e-24, -6.86e-25, 8.18e-4, -8.26e-2, 8.62e-23, -2.68e-23, -3.83e-23, -6.18e-24  
0, 0  
-4.78e-2, 1.49e-2, 1.55, 2.81e-2, 1.92e-2, -2.95e-7, 0, 0, 0, 1.71e+1, 6.34e-1, 2.29e-2, -2.95e-3, 1.92e-4, 9.88e-4, 3.58e-7, -4.07e-7, 1.25e-1, -2.73e-1, 9.19e-3, 2.2e-2  
0, 0  
-1.59e-1, 5.85e-1, -1.05e-2, 2.33, 1.72, 3.71e-5, 0, 0, 0, 4.78e-2, -2.09e-3, 1.71e+1, 6.34e-1, 6.35e-1, -1.57e-4, -4.56e-5, 5.17e-5, 5.08e-2, 4.46e-2, 1.27e-1, -3.35e-1  
0, 0  
5.85e-1, 1.7e-1, -7.08e-3, 1.72, -2.34, -2.03e-3, 0, 0, 0, 5.81e-3, -4.76e-4, -6.35e-1, 6.82e-4, 1.71e+1, 6.35e-1, 1.84e-4, 6.36e-5, 1.1e-2, 5.11e-2, 3.35e-1, -3.93e-3  
0, 0  
7.6e-25, 1.64e-23, 5.3e-22, 8.49e-23, -1.56e-22, -2.39e-26, 0, 0, 0, -2.11e-21, -2.37e-24, -4.84e-22, 4.23e-23, -6.25e-23, -1.44e-23, 1.71e+1, 6.34e-1, -3.81e-21, -5.62e-21, -7.66e-24, -5.05e-24  
0, 0  
-4.48e-2, 1.57e-2, 1.55, 8.85e-3, 3.15e-2, -2.91e-6, 0, 0, 0, -1.41e+1, -1.65, -6.76e-2, -1.97e-3, -1e-2, 4.9e-5, -4.34e-9, 4.27e-7, 2.72e-1, -1.5e-1, 6.02e-3, 1.88e-2  
0, 0  
-1.83e-1, 1.29e-2, -1.21e-2, 1.87, 2.68, 3.75e-5, 0, 0, 0, -1.35e-1, -9.04e-3, -1.41e+1, -1.65, -1.65, -2.63e-4, -4.68e-5, 5.32e-5, 9.19e-2, 3.7e-2, 2.64e-1, -2.17e-1  
0, 0  
1.35e-2, 1.95e-1, -3.99e-4, 2.68, -1.89, -2.09e-3, 0, 0, 0, -1.39e-2, -2.99e-3, 1.64, 6.15e-4, -1.41e+1, -1.65, 1.89e-4, 6.53e-5, 1.85e-2, 7.15e-2, 2.17e-1, -3.97e-3  
0, 0  
-2.27e-23, 7.4e-23, 7.41e-22, 3.35e-22, 1.98e-22, -2.65e-26, 0, 0, 0, 9.63e-21, 5.82e-22, 1.96e-21, 5.42e-23, 3.04e-22, -4.07e-24, -1.41e+1, -1.65, -8.82e-21, -8.25e-21, -3.13e-24, -1.75e-23

(34)





-1.22e-5, 1e-4, 1.83e-4, -1.28e-3, -5.46e-3, -2.45e-7, 0, -1.79e-3, 0, 1.28e-5, -8.94e-5, -3.05e-4, -1.18e-4, -1.09e-4, -2.07e-4, -1.54e-6, -4.21e-6, -5e-5, -1.49e-4, 1.64e-4, 2.29e-2  
-9.01e-5, -2.8e-3, -5.72e-5, 5.57e-3, -1.22e-3, -1e-1, 1.79e-3, 3.88e-7, 0, -6.26e-5, -5.52e-4, -1.03e-4, -1.8e-4, 4.19e-4, 1.16e-4, -2.59e-6, -4.73e-6, -1.76e-4, -1.41e-5, 6.58e-3, -2.09e-5  
6.01e-4, -2.58e-6, -2.65e-3, 4.25e-4, 1.02e-1, 2.46e-7, 7.28e-6, -9.55e-5, 0, -4.37e-3, 3.33e-4, -1.34e-4, -2.36e-5, 2.66e-5, 3.68e-5, -5.87e-8, -4.65e-8, -3.52e-7, 3.31e-3, 3.67e-4, 1.43e-3  
-6.9e-4, 1.34e-2, 1.24e-3, 2.17e-3, -1.04e-2, -7.39e-3, 0, 0, 0, -6.61e-5, -5.05e-3, -9.89e-4, 2.03e-4, -1.71e-2, 3.16e-4, 2.43e-4, 2.13e-4, 6.47e-3, -6.41e-4, 6.39e-2, -3.46e-3  
4.35e-3, -4.27e-4, -1.6e-2, 4.1e-3, -7.93e-3, 5.5e-7, 0, 0, 0, -1.07e-4, -3.07e-4, -5.02e-3, 1.95e-4, 4.22e-4, -1.51e-4, -1.5e-4, -1.17e-4, 2.8e-4, 4.16e-4, -9.68e-4, -6.42e-2  
-1.92e-4, 2.46e-2, 1.06e-4, -1.82e-3, 1.67e-3, -1.45e-2, 0, 0, 0, 2.91e-5, -4.45e-4, -3.68e-4, 1.74e-5, -1.62e-3, 2.72e-5, 4.94e-5, 1.84e-5, 2.18e-2, 2.57e-3, 6.34e-3, -2.85e-4  
0, 0, 0, 1, -2.17e-4, 5.33e-2, 7.67e-22, 7.83e-20, 0  
0, 0, 0, 0, 1, 4.07e-3, -7.81e-20, 0  
0, 0, 0, 0, -4.07e-3, 1, 1.44e-20, 4.17e-21, 0, 0, 0, 0, 0, 0, 0, 0, 0, 0, 0, 0, 0, 0, 0, 0, 0, 0, 0  
0, 0, 0, 0, 0, 0, 0, 0, 0, 1, 0, 0, 0, 0, 0, 0, 0, 0, 0, 0, 0, 0, 0, 0  
2.87e-2, 3.39e-2, 1.56, 8.98e-2, 3.79e-4, -1.29e-5, 0, 0, 0, -7.79, -9.31e-1, -6.24e-3, 1.44e-3, 5.57e-3, -8.03e-2, -3.63e-6, -2.79e-6, 1.92e-2, -9.22e-3, -9.92e-3, 4.06e-2  
0, 0, 0, 0, 0, 0, 0, 0, 0, 0, 0, 0, 0, 0, 0, 0, 1, 0, 0, 0, 0, 0, 0, 0  
-7.28e-2, 4.51e-1, -2.19e-2, 2.06, 4.42e-1, 1.32e-4, 0, 0, 0, -1.73e-1, 1.14e-3, -6.79, -9.3e-1, -9.48e-1, -2, -1.64e-4, -1.28e-4, -2.56e-2, 8.32e-2, 1.84e-2, -1.02e-1  
0, 0, 0, 0, 0, 0, 0, 0, 0, 0, 0, 0, 0, 0, 0, 0, 0, 1, 0, 0, 0, 0, 0, 0  
3.83e-1, 1.09e-1, 7.17e-1, 4.58e-1, -2.05, -7.87e-3, 0, 0, 0, 7.29e-3, -1.65e-1, 9.1e-1, 2, -6.81, -9.3e-1, 2.56e-4, 2.25e-4, 1.17e-2, -2.16e-2, 8.84e-2, -6.9e-3  
0, 0  
7.12e-33, -8.43e-32, -5.46e-32, -3.24e-31, -1.35e-31, 1.13e-35, 0, 0, 0, 3.7e-31, 5.72e-32, 6.19e-34, 6.74e-32, 1.32e-31, -6.97e-34, -7.79, -9.3e-1, 5.26e-31, 2.15e-30, 3.31e-34, 8.97e-32  
0, 1, 0, 0  
-1.39e-2, 1.23e-3, 3.9e-2, -2.97e-2, 4.98e-2, -1.86e-4, 0, 0, 0, -3.64e-4, -6.29e-2, -1.02e-2, -2.32e-2, 2.26e-4, 1.15e-2, 6.09e-6, 5.35e-6, -3.86e-1, -6.3e-2, -6.25e-3, -1.51e-3  
0, 1  
-2.86e-3, 5.8e-2, -6.82e-3, 7.16e-3, 1.85e-2, -4.27e-3, 0, 0, 0, -3.83e-3, -4.9e-2, -2.37e-4, -8.18e-2, -9.16e-2, 1.15e-3, 1.389e-4, 1.22e-4, -1.05e-2, -3.48e-3, 6.46e-1, -6.48e-2  
0, 0  
4e-2, 3.09e-3, -6.36e-2, 1.69e-2, -3.92e-3, -7.53e-5, 0, 0, 0, 4.88e-2, 2.19e-2, 8.52e-2, 4.34e-4, 1.1e-3, -8.17e-2, 8.93e-5, 6.97e-5, -2.09e-3, 1.81e-2, 6.31e-2, 2.04  
0, 0  
3.44e-32, 2.18e-32, -1.24e-31, -2.13e-32, 3.47e-31, -2.69e-38, 0, 0, 0, 5.7e-32, -1.14e-30, -3.59e-34, -1.13e-31, -1.13e-31, -4.24e-34, 9.65e-4, -8.19e-2, -9.42e-32, 3.17e-32, 5.44e-32, -2.43e-32  
0, 0  
-2.85e-1, 2.63e-2, 1.55, 1.31e-1, 1.11e-1, 3.83e-6, 0, 0, 0, 1.71e+1, 6.33e-1, 1.64e-1, -5.81e-3, -9.41e-3, 3.47e-3, 2.1e-6, 1.63e-6, 1.2e-1, -2.69e-1, -4.1e-2, 4.29e-2  
0, 0  
-1.53e-1, 4.48e-1, -1.63e-2, 2.33, 1.71, 1.32e-4, 0, 0, 0, 3.35e-1, -3.86e-3, 1.71e+1, 6.32e-1, 6.61e-1, 9.99e-4, -1.52e-4, -1.19e-4, 6.4e-2, 8.91e-2, 1.21e-1, -3.08e-1  
0, 0  
4.84e-1, 1.59e-1, -3.69e-1, 1.71, -2.33, -7.3e-3, 0, 0, 0, -9.24e-3, 5.29e-4, -6.05e-1, 6.31e-4, 1.71e+1, 6.33e-1, 2.38e-4, 2.09e-4, 8.67e-3, 1.63e-1, 3.15e-1, -6.31e-3  
0, 0  
-6.17e-32, -8.31e-32, -4.49e-31, 1.12e-31, 7e-31, 2.09e-34, 0, 0, 0, 1.22e-30, -1.17e-32, 7.31e-31, -5.71e-32, -1e-31, 4.39e-32, 1.71e+1, 6.32e-1, 2.89e-30, 3.96e-30, 3.83e-32, 2e-31  
0, 0  
-1.36e-1, 1.55e-2, 1.55, 9.03e-2, 8.6e-2, 1.85e-5, 0, 0, 0, -1.41e+1, -1.65, -1.98e-1, -3.72e-3, 9.82e-3, 9.72e-4, -2.83e-6, -2.26e-6, 2.26e-1, -1.5e-1, -2.19e-2, 3.26e-2  
0, 0  
-1.39e-1, 1.02e-2, -2.81e-2, 1.8, 2.65, 1.3e-4, 0, 0, 0, -3.94e-1, -1.81e-2, -1.42e+1, -1.65, -1.66, -2.68e-5, -1.57e-4, -1.23e-4, 2.09e-1, 6.34e-2, 2.26e-1, -2.33e-1  
0, 0  
-5.73e-3, 1.67e-1, 1.85e-1, 2.67, -1.82, -7.53e-3, 0, 0, 0, 3.16e-2, -2.38e-3, 1.64, 6.17e-4, -1.41e+1, -1.65, 2.45e-4, 2.15e-4, -3.91e-2, 2.48e-1, 2.31e-1, -6.95e-3  
0, 0  
9.16e-32, -1.1e-31, -4.86e-31, -4.27e-31, -7.91e-31, -8.87e-35, 0, 0, 0, -6.62e-30, -3.93e-31, -3.04e-30, -7.76e-32, 2.21e-31, 2.15e-32, -1.41e+1, -1.65, 6.26e-30, 5.27e-30, -2.83e-32, 6.91e-32

40kts  $\xi =$

(36)



$$\begin{aligned}
 \mathbf{1kt} \mathbf{B}_p = & \begin{bmatrix} 7.16e-6, 1.34e-4, 1.12e-6, 1.17e-9 \\ -7.4e-6, 4.7e-7, -1.27e-4, 2.46e-4 \\ 2.94e-5, -1.98e-5, -3.59e-6, 1.44e-8 \\ 1.8e-5, 1.3e-4, -1.03e-3, 8.8e-4 \\ 2.49e-6, -3.16e-4, -3.86e-5, -2.19e-8 \\ 8.99e-7, 1.41e-5, 1.97e-7, -3.74e-3 \\ 0, 0, 0, 0 \\ 0, 0, 0, 0 \\ 0, 0, 0, 0 \\ 0, 0, 0, 0 \\ 0, 0, 0, 0 \\ 3.91e-1, 1e-3, 1.82e-3, 1.46e-6 \\ 0, 0, 0, 0 \\ 2.09e-3, 3.9e-1, -1.18e-5, -1.56e-5 \\ 0, 0, 0, 0 \\ 3.58e-3, 1.38e-4, 3.9e-1, 9.34e-4 \\ 0, 0, 0, 0 \\ -3.42e-24, 6.54e-25, -5.6e-25, 4.16e-28 \\ 0, 0, 0, 0 \\ 9.18e-2, 1.57e-3, -1.46e-2, 1.08e-5 \\ 0, 0, 0, 0 \\ 3.66e-03, 9.18e-2, -5.7e-4, 5.08e-4 \\ 0, 0, 0, 0 \\ -2.94e-2, 2.05e-4, 9.16e-2, 8.86e-6 \\ 0, 0, 0, 0 \\ 6.49e-24, -6.04e-26, -2.56e-24, -4.38e-29 \\ 0, 0, 0, 0 \\ 1.63, 3.69e-3, 5e-4, 1.27e-7 \\ 0, 0, 0, 0 \\ 7.12e-3, 1.63, -3.16e-5, -1.60e-5 \\ 0, 0, 0, 0 \\ 1.28e-3, 1.12e-4, 1.62, 8.76e-4 \\ 0, 0, 0, 0 \\ 1.08e-22, 2.76e-23, 1.51e-24, 1.03e-26 \\ 0, 0, 0, 0 \\ 2.56, 1.5e-3, -8.17e-4, 1.26e-6 \\ 0, 0, 0, 0 \\ 3.3e-3, 2.56, -1.93e-4, -1.62e-5 \\ 0, 0, 0, 0 \\ -1.88e-3, -5.5e-5, 2.56, 9.01e-4 \\ 0, 0, 0, 0 \\ 8.35e-22, 1.65e-22, 3.06e-23, 1.14e-26 \end{bmatrix}, \quad
 \mathbf{40kts} \mathbf{B}_p = \begin{bmatrix} 2.09e-5, 9.14e-5, -1.89e-5, 2.8e-9 \\ -6.34e-6, -2.23e-5, -7.94e-5, 2.46e-4 \\ -5.18e-6, -4.11e-5, -1.04e-5, -2.92e-8 \\ 8.08e-5, -2.05e-4, -3.92e-4, 8.8e-4 \\ -5.76e-6, -1.47e-4, 5.5e-5, -2.62e-8 \\ 1.46e-6, 4.26e-5, 1.54e-4, -3.74e-3 \\ 0, 0, 0, 0 \\ 0, 0, 0, 0 \\ 0, 0, 0, 0 \\ 0, 0, 0, 0 \\ 0, 0, 0, 0 \\ 4.28e-1, -6.56e-4, 1.59e-1, 1.54e-6 \\ 0, 0, 0, 0 \\ -1.26e-3, 4.1e-1, 2.88e-4, -1.57e-5 \\ 0, 0, 0, 0 \\ 3.18e-1, -1.12e-5, 4.45e-1, 9.37e-4 \\ 0, 0, 0, 0 \\ -5.88e-34, -1.32e-31, 1.35e-33, -1.35e-36 \\ 0, 0, 0, 0 \\ 9.14e-2, 3.4e-3, -2.24e-2, 2.22e-5 \\ 0, 0, 0, 0 \\ 7.68e-3, 9.64e-2, -2.55e-5, 5.08e-4 \\ 0, 0, 0, 0 \\ -4.56e-2, 2.49e-4, 8.6e-2, 8.94e-6 \\ 0, 0, 0, 0 \\ -7.21e-33, 1.24e-31, 1.63e-32, 3.22e-39 \\ 0, 0, 0, 0 \\ 1.61, 3.99e-3, 1.53e-1, -4.56e-7 \\ 0, 0, 0, 0 \\ 7.89e-3, 1.62, -1.61e-4, -1.57e-5 \\ 0, 0, 0, 0 \\ 3.07e-1, 9.87e-4, 1.6, 8.69e-4 \\ 0, 0, 0, 0 \\ -7.05e-32, -1.77e-31, -3.1e-32, -2.49e-35 \\ 0, 0, 0, 0 \\ 2.56, 3.55e-4, 1.5e-1, -2.2e-6 \\ 0, 0, 0, 0 \\ 8.75e-4, 2.56, -4.04e-4, -1.55e-5 \\ 0, 0, 0, 0 \\ 3.01e-1, 9.28e-4, 2.57, 8.96e-4 \\ 0, 0, 0, 0 \\ -5.47e-31, -3.78e-31, -3.78e-32, 1.06e-35 \end{bmatrix}, \quad
 \mathbf{x}_p = \begin{bmatrix} u \\ v \\ w \\ p \\ q \\ r \\ \phi_A \\ \theta_A \\ \psi_A \\ \beta_0 \\ \dot{\beta}_0 \\ \beta_c \\ \dot{\beta}_c \\ \beta_s \\ \dot{\beta}_s \\ \beta_d \\ \dot{\beta}_d \\ \zeta_0 \\ \dot{\zeta}_0 \\ \zeta_c \\ \dot{\zeta}_c \\ \zeta_s \\ \dot{\zeta}_s \\ \zeta_d \\ \dot{\zeta}_d \\ 2\beta_0 \\ 2\dot{\beta}_0 \\ 2\beta_c \\ 2\dot{\beta}_c \\ 2\beta_s \\ 2\dot{\beta}_s \\ 2\beta_d \\ 2\dot{\beta}_d \\ 3\beta_0 \\ 3\dot{\beta}_0 \\ 3\beta_c \\ 3\dot{\beta}_c \\ 3\beta_s \\ 3\dot{\beta}_s \\ 3\beta_d \\ 3\dot{\beta}_d \end{bmatrix}, \quad
 \mathbf{u} = \begin{bmatrix} \theta_0 \\ \theta_c \\ \theta_s \\ \theta_T \end{bmatrix} \quad (38)
 \end{aligned}$$